

General circulation model estimates of aerosol transport and radiative forcing during the Indian Ocean Experiment

M. Shekar Reddy,¹ O. Boucher,¹ C. Venkataraman,² S. Verma,² J.-F. Léon,¹ N. Bellouin,¹ and M. Pham³

Received 21 January 2004; revised 10 May 2004; accepted 3 June 2004; published 20 August 2004.

[1] Aerosol sources, transport, and sinks are simulated, and aerosol direct radiative effects are assessed over the Indian Ocean for the Indian Ocean Experiment (INDOEX) Intensive Field Phase during January to March 1999 using the Laboratoire de Météorologie Dynamique (LMDZT) general circulation model. The model reproduces the latitudinal gradient in aerosol mass concentration and optical depth (AOD). The model-predicted aerosol concentrations and AODs agree reasonably well with measurements but are systematically underestimated during high-pollution episodes, especially in the month of March. The largest aerosol loads are found over southwestern China, the Bay of Bengal, and the Indian subcontinent. Aerosol emissions from the Indian subcontinent are transported into the Indian Ocean through either the west coast or the east coast of India. Over the INDOEX region, carbonaceous aerosols are the largest contributor to the estimated AOD, followed by sulfate, dust, sea salt, and fly ash. During the northeast winter monsoon, natural and anthropogenic aerosols reduce the solar flux reaching the surface by 25 W m^{-2} , leading to 10–15% less insolation at the surface. A doubling of black carbon (BC) emissions from Asia results in an aerosol single-scattering albedo that is much smaller than in situ measurements, reflecting the fact that BC emissions are not underestimated in proportion to other (mostly scattering) aerosol types. South Asia is the dominant contributor to sulfate aerosols over the INDOEX region and accounts for 60–70% of the AOD by sulfate. It is also an important but not the dominant contributor to carbonaceous aerosols over the INDOEX region with a contribution of less than 40% to the AOD by this aerosol species. The presence of elevated plumes brings significant quantities of aerosols to the Indian Ocean that are generated over Africa and Southeast and east Asia. **INDEX TERMS:** 0305 Atmospheric Composition and Structure: Aerosols and particles (0345, 4801); 0368 Atmospheric Composition and Structure: Troposphere—constituent transport and chemistry; 0345 Atmospheric Composition and Structure: Pollution—urban and regional (0305); 0360 Atmospheric Composition and Structure: Transmission and scattering of radiation; **KEYWORDS:** Indian Ocean, India, south Asia, radiative impacts, fly ash

Citation: Reddy, M. S., O. Boucher, C. Venkataraman, S. Verma, J.-F. Léon, N. Bellouin, and M. Pham (2004), General circulation model estimates of aerosol transport and radiative forcing during the Indian Ocean Experiment, *J. Geophys. Res.*, 109, D16205, doi:10.1029/2004JD004557.

1. Introduction

[2] It has now been established that anthropogenic activities have increased significantly the concentrations of atmospheric aerosols. Biomass and fossil fuel combustion results in primary aerosols (e.g., black carbon, organic carbon, and fly ash) and aerosol precursor gases (e.g., SO_2 , NH_3 , NO_x , and volatile organic compounds). Natural emissions of windblown dust, sea salt, dimethylsulfide

(DMS), and volatile organic compounds (VOCs) also contribute to atmospheric aerosols. Sulfate and sea salt scatter solar radiation and exert a negative radiative forcing while black carbon (BC) mostly absorbs solar radiation, heating the atmosphere and further cooling the Earth's surface. Some aerosol types, such as mineral dust and organic carbon (OC), both scatter or absorb solar radiation depending on the particle size and composition.

[3] During the Indian winter monsoon, from roughly December to March, dry and polluted continental air masses from south and Southeast Asia are transported across the Bay of Bengal and the Arabian Sea to the equatorial Indian Ocean and are mixed with air masses from the Southern Hemisphere, forming a gigantic natural laboratory to understand aerosol climate interactions. The objectives of the Indian Ocean Experiment (INDOEX) were to understand the nature and magnitude of the chemical pollution

¹Laboratoire d'Optique Atmosphérique, CNRS, Université des Sciences et Technologies de Lille, Villeneuve d'Ascq, France.

²Department of Chemical Engineering, Indian Institute of Technology Bombay, Mumbai, India.

³Service d'Aéronomie, Université Pierre et Marie Curie, Paris, France.

over the Indian Ocean and relative importance of sulfate, carbonaceous, and other aerosols for the direct and indirect radiative effects [Ramanathan *et al.*, 2001]. During the northeast winter monsoon periods between 1995 and 1999 a number of field experiments were carried out culminating in an Intensive Field Phase in 1999 (IFP99). Vast amounts of data were collected from different platforms about trace gases, aerosols, clouds, and radiation.

[4] The measured aerosol concentrations, particularly BC, were larger during IFP99 than observed in other parts of the world [Dickerson *et al.*, 2002; Chowdhury *et al.*, 2001; Neusiß *et al.*, 2002]. By examining OC to BC ratios from aircraft measurements, Novakov *et al.* [2000] concluded that fossil fuel combustion is the major source of absorbing aerosols. Mayol-Bracero *et al.* [2002] reached a similar conclusion although their tentative emission estimates for BC indicate the opposite. In contrast, Guazzotti *et al.* [2003] using single particle analysis concluded that biomass burning is the main source of aerosols over the INDOEX region. Satheesh and Srinivasan [2002] estimated the contribution of different species to the total aerosol optical depth (AOD) by combining measured AODs and surface mass concentrations. They estimated the contribution of natural aerosols (sea salt and mineral dust) to be more than 50% for the period of May to September. Bottom-up emission inventories from fuel consumption and pollutant emission factors for India [Reddy and Venkataraman, 2002a, 2002b; Habib *et al.*, 2004] and Asia [Streets *et al.*, 2003] suggest the dominance of fossil fuel sources for sulfur emissions and biomass sources for carbonaceous aerosol emissions. Although aerosols have been extensively characterized over the INDOEX region, the issue of source attribution is still not resolved. Simulations of the atmospheric cycling of aerosols using a global transport model, as done in this study, are therefore a necessary step toward source apportionment.

[5] There are only few aerosol modeling studies pertaining to the INDOEX-IFP99 [Rasch *et al.*, 2001; Collins *et al.*, 2002; Minvielle *et al.*, 2004a, 2004b]. Rasch *et al.* [2001] and Collins *et al.* [2002] used the MATCH model and assimilated AOD from satellite measurements. However, it was not possible to use the satellite information to discriminate between the different aerosol species so the relative contributions of each species were the same before and after the assimilation procedure. Rasch *et al.* [2001] also assessed the contribution of different geographical regions to aerosol loads over the Indian Ocean by prescribing constant radon emission fluxes. As the aerosol emission distributions and injection heights differ for different sources and regions this approach yields only a qualitative estimate of regional contributions. In a recent study using the Laboratoire de Météorologie Dynamique (LMDZT) general circulation model (GCM) at a very high resolution, S. Verma *et al.* (manuscript in preparation, 2004) demonstrated how aerosols could be lofted and transported over the Arabian Sea during events of sea breeze along the west coast of India in an overall northwesterly flow.

[6] The present study is similar in some aspects to that of Rasch *et al.* [2001] and Collins *et al.* [2002] but also presents many differences. We employ a GCM in zoom mode over the INDOEX region with an increased spatial resolution of about $1^\circ \times 1^\circ$. Aerosol emission sources near

the source regions correspond to the campaign period with a finer source classification and spatial resolution. In addition, global open biomass-burning emissions have a seasonality deduced from satellite measured fire counts. The specific objectives of the present study are (1) to estimate aerosol distribution and optical depth, (2) to assess the relative contribution of different aerosol species to the estimated AOD, (3) to assess the aerosol shortwave direct radiative forcing and the atmospheric absorption of solar radiation, and (4) to quantify the contribution of South Asia to the aerosol loadings over the INDOEX region.

2. Model Description and Setup

[7] Our global multicomponent aerosol model has been described in previous studies. Sulfate formation, transport, and radiative forcing were described by Boucher *et al.* [2002] and Boucher and Pham [2002]. The atmospheric cycle of carbonaceous aerosols was studied by Reddy and Boucher [2004]. Sea salt generation and related radiative forcing are discussed by O. Boucher *et al.* (manuscript in preparation, 2004). Finally, M. S. Reddy *et al.* (Global multi-component aerosol optical depths and radiative forcing estimates in the LMDZT general circulation model, submitted to *Journal of Geophysical Research*, 2004) (hereinafter referred to as Reddy *et al.*, submitted manuscript, 2004) described the global multicomponent aerosol optical depths and estimates of the direct radiative forcing. Here we do not repeat the full description of the model but give only a summary of its salient features.

2.1. Atmospheric Transport

[8] Atmospheric transport is computed with a finite volume transport scheme for large-scale advection [van Leer, 1977; Hourdin and Armangaud, 1999], a scheme for turbulent mixing in the boundary layer, and a mass flux scheme for convection [Tiedtke, 1989]. The model has a resolution of 96 points in longitude and 72 points in latitude, with 19 vertical layers of a hybrid sigma-pressure coordinate. The average height of the lowest model layer is about 150 m. We use the model in zoom mode with the zoom centered at 75°E and 15°N and zoom factors of 4 and 3, resulting in a resolution of about 1° in longitude and 0.8° in latitude, respectively, over the INDOEX domain (Figure 1). The time step is 1 min for resolving the dynamical part of the primitive equations. Mass fluxes are cumulated over five time steps so that large-scale advection is applied every 5 min. The physical and chemical parameterizations are applied every 30 time steps or 30 min. The different processes are handled through operator splitting.

2.2. Aerosol Emissions

[9] The global sulfur dioxide (SO_2) emissions are from the EDGAR database (version 3.2) [Olivier and Berdowski, 2001] for fossil fuel combustion and industrial processes for the base year 1995. The sulfur emissions from biomass-burning and natural (volcanic and biogenic) sources are as described by Boucher *et al.* [2002]. A fixed 5% of sulfur emissions from combustion sources is assumed to be emitted as sulfate and with remaining 95% in the form of SO_2 . The carbonaceous aerosol emissions are the same as those given by Reddy and Boucher [2004], which include

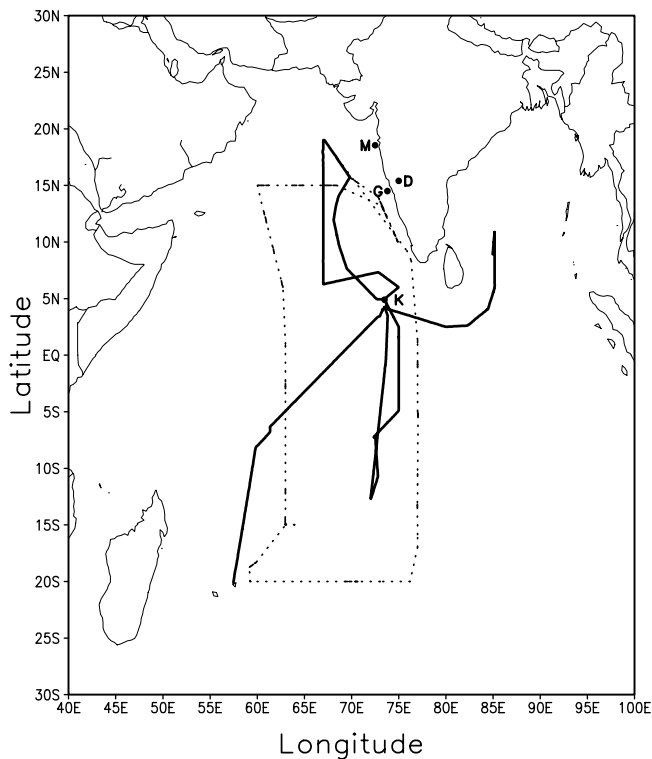


Figure 1. Indian Ocean Experiment (INDOEX) region. Solid and dotted lines indicate tracks of the *Ronald Brown* and *Sagar Kanya* cruises, respectively. Capital letters G, D, K, and M mark the locations of Goa, Dharwar, the Kaashidhoo Climate Observatory (KCO), and Mumbai/Bombay.

emissions from fossil fuel combustion and biomass burning, and natural biogenic sources. The seasonal to interannual variability of open biomass-burning emissions was inferred from ATSR satellite fire counts. Sea salt emissions are parameterized as a function of horizontal wind speed at 10-m height using the source formulation from *Monahan et al.* [1986]. The size range corresponds to particle radius (at 80% relative humidity) between 0.045 and 20 μm in 10 size bins (O. Boucher et al., manuscript in preparation, 2004). Monthly mean dust emission fluxes from natural and anthropogenic sources are prescribed from *Tegen and Fung* [1995]. Dust emissions are split between submicron and supermicron size ranges.

[10] Emissions of SO_2 , BC, and OC from fossil fuel and biomass sources over south, Southeast, and east Asia are from *Streets et al.* [2003]. Hereafter we refer to these regions as “Asia” for the sake of convenience. These estimates are from a fine source classification and emission factors representative of Asia for the base year 2000. Asian emissions are nested into the global emission maps.

[11] Over the Indian region we use the emissions of *Reddy and Venkataraman* [2002a, 2002b] with a resolution of $0.25^\circ \times 0.25^\circ$ for biomass- and fossil-fuel-burning sources. The above emissions do not include emissions from crop waste burning in the fields, for which the separate estimates of *Reddy et al.* [2002] are used.

[12] Oxygen, hydrogen, and other chemical species are always associated with OC, and the resulting aerosol is

called organic matter (OM). We use an OM to OC ratio of 1.4 and 1.6, for fossil fuel and biomass sources, respectively [*Turpin and Lim*, 2001; *Reddy and Boucher*, 2004]. We assume that BC emissions occur as 80% hydrophobic and 20% hydrophilic, whereas OM emissions occur as 50% hydrophobic and hydrophilic. The aging of BC and OM from hydrophobic to hydrophilic form in the atmosphere is represented by an exponential lifetime of 1.63 days [*Reddy and Boucher*, 2004]. The fossil fuel emissions from large point sources (LPS) are released in the second model layer to account for the tall stacks. Over Asia, carbonaceous aerosol emissions from LPS are also released in the model second layer. A fraction of open biomass-burning emissions are known to reach higher altitudes because of thermal convection. We therefore emit them in model layers 3 to 5, corresponding roughly to heights ranging from 350 to 1500 m [*Reddy and Boucher*, 2004].

2.3. Aerosol Deposition

[13] Aerosol dry deposition is estimated from the concentration in the lowest model layer and a prescribed dry deposition velocity. In addition to dry deposition, sea salt and dust are deposited through sedimentation because of their large particle size. Aerosol sedimentation is parameterized using Stoke’s law. Changes in particle size and mass density with relative humidity (RH) are accounted for in the calculation of sedimentation velocities for sea salt. Wet deposition (or scavenging) is treated separately for stratiform and convective precipitation and differently for different aerosols. In-cloud scavenging is parameterized similarly to *Giorgi and Chameides* [1986]. The fraction of chemical species in the aqueous phase vary for different aerosol types. The hydrophobic carbonaceous aerosols are not allowed to be deposited through in-cloud scavenging. Below-cloud scavenging is parameterized by integrating over the population of raindrops the volume of space that is swept by a raindrop during its fallout. Below-cloud scavenging is applied to both hydrophobic and hydrophilic carbonaceous aerosols in the same manner. In addition, a fraction of the soluble tracers (χ) is scavenged in the convective transport. The aerosol deposition parameterization is detailed by *Reddy et al.* (submitted manuscript, 2004) and *Boucher et al.* [2002].

2.4. Aerosol Optical Properties and Radiative Forcing

[14] The radiative code in the LMDZT GCM consists of improved versions of the parameterizations of *Fouquart and Bonnel* [1980] (solar radiation) and *Morcrette* [1991] (terrestrial radiation). The shortwave spectrum is divided into two intervals: 0.25–0.68 and 0.68–4.00 μm . The shortwave radiative fluxes are computed every two hours with and without the presence of clouds, and with and without the presence of aerosols at the top-of-atmosphere (TOA) and at the surface. The clear-sky and all-sky aerosol radiative forcing can then be estimated as the differences in shortwave radiative fluxes with and without aerosols.

[15] Aerosol optical properties (mass extinction efficiency, α_e , single-scattering albedo, ω , and asymmetry factor, g) for all aerosol species are computed using Mie theory with prescribed size distributions and refractive indices. In the absence of reliable optical properties for fly ash we use those of submicron mineral dust. Optical properties were computed

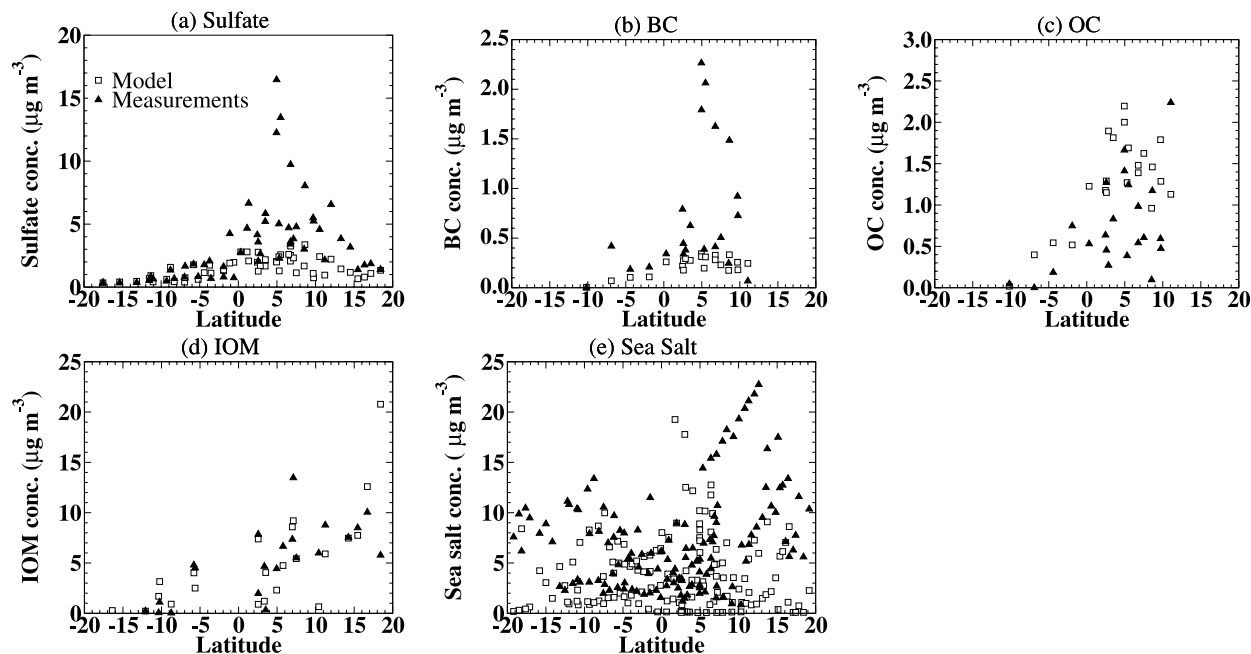


Figure 2. Aerosol mass concentrations as a function of latitude for the *Ronald Brown* cruise during INDOEX-IFP99 for (a) sulfate, (b) BC, (c) OC, (d) IOM, and (e) sea salt. Measurements are indicated by triangles. The model results are sampled along the cruise track with a resolution of 6 hours and are indicated by squares. The sum of model dust and fly ash is compared with measured IOM concentrations.

over the entire shortwave spectrum (0.25–4.0 μm) at 24 wavelengths and grouped into the two model wavebands as weighted averages with a typical spectral distribution of the incoming solar radiation flux at the surface. We also consider the RH affects on both particle size and density of sulfate, hydrophilic OM, and sea salt. Further details on our parameterization of aerosol optical properties are given by Reddy et al. (submitted manuscript, 2004).

2.5. Experiments

[16] Horizontal model winds were nudged to 6 hourly winds from ECMWF analyses with a relaxation time of 0.1 days [Hauglustaine et al., 2004]. This ensures that the model transport is reasonably constrained by ECMWF meteorology while other dynamical and physical processes are driven by the model parameterizations. Simulations in nudged mode allow a fair comparison of modeled parameters with field campaign measurements. Simulations were carried out for the period of January to March 1999, after two months of spin-up.

3. Model Evaluation

[17] Aerosol concentrations and optical depths at the global scale were evaluated in previous studies [Boucher et al., 2002; Boucher and Pham, 2002; Reddy and Boucher, 2004; Reddy et al., submitted manuscript, 2004; O. Boucher et al., manuscript in preparation, 2004]. Model-predicted aerosol mass concentrations and AODs are now compared with measurements made from different platforms during IFP99. The focus area of the campaign was the Arabian Sea and the Indian Ocean. Measurements were made from two research vessels (*Ronald Brown* and *Sagar Kanya*), three

aircrafts, and two field stations in the Indian Ocean located at Kaashidhoo (4.9°N, 73.5°E) and Malé (4.1°N, 73.3°E). There were also ground stations located over continental India including Goa (15.5°N, 73.8°E), Dharwar (15.4°N, 75.0°E), and Bombay (18.6°N, 72.5°E) [Ramanathan et al., 2001]. A map of the INDOEX region indicating ship tracks and the ground measurement sites is shown in Figure 1.

[18] The *Ronald Brown* cruised in the INDOEX region from January to March. Size resolved aerosol mass concentrations and AODs were measured onboard [Quinn et al., 2002]. The model aerosol concentrations are sampled from a 6 hourly average output along the cruise path and compared with measurements (Figure 2). The measured inorganic oxidized matter (IOM) was compared with the sum of modeled dust and fly ash (Figure 2d). Aerosol concentrations are smaller in the southern Indian Ocean (SIO) and the ITCZ with largest values along the west coast of India. The model captures the north to south gradient in measured concentrations with smaller values over the SIO and ITCZ and larger values over the Arabian Sea. However, over the region of largest concentrations (5°–10°N), modeled sulfate and BC concentrations are a factor of 2 to 3 lower than measured values.

[19] Modeled surface mass concentrations are compared with reported measurements [Chowdhury et al., 2001; Rasch et al., 2001] in Figure 3. Modeled sulfate concentrations are at the lower end of the measurements. The BC and dust concentrations are underestimated by a factor of 2 to 4 for the entire period (Figures 3b and 3d). There is a better agreement between the model and measurements for OC and sea salt (Figures 3c and 3e).

[20] A comparison of modeled AOD (at 670 nm) with measurements onboard the *Ronald Brown* and *Sagar Kanya*

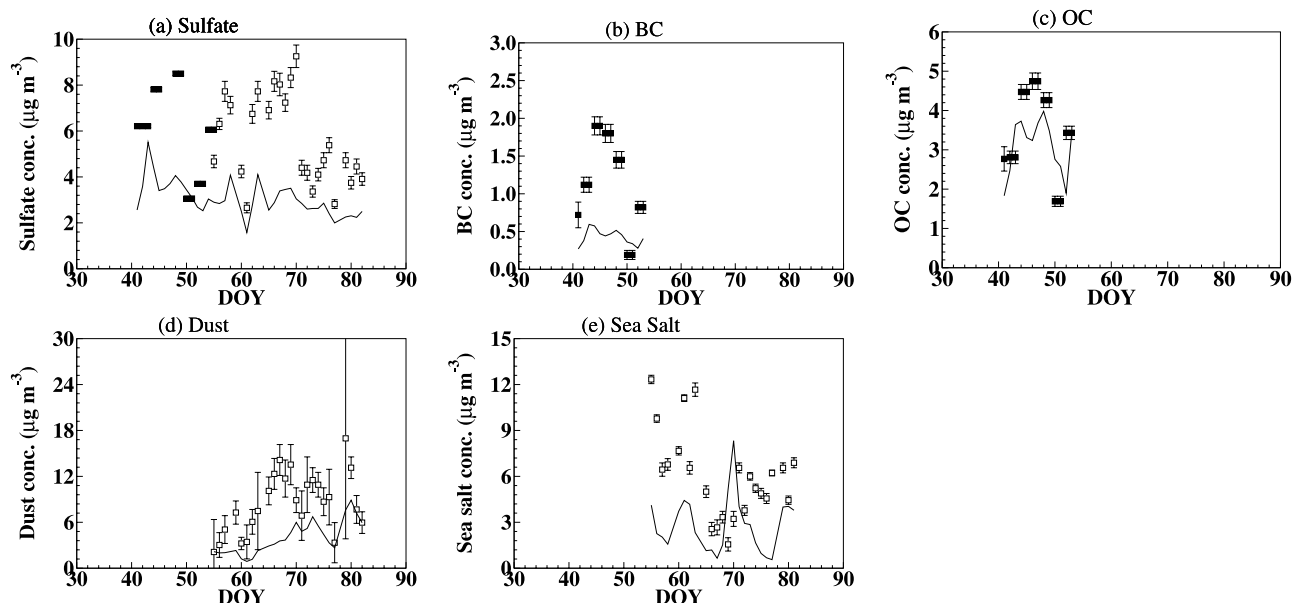


Figure 3. Modeled (solid lines) and measured (symbols) surface aerosol concentrations at KCO: (a) sulfate, (b) BC, (c) OC, (d) dust, and (e) sea salt. Data shown as solid and open squares are from Chowdhury *et al.* [2001] and D. Savoie and J. Prospero (as reported by Rasch *et al.* [2001]), respectively.

is shown in Figure 4. AODs are smaller in the ITCZ, moderate over the SIO, and largest over the Arabian Sea. The model agrees relatively well with measurements except at latitudes 5° – 15° N where the model values are lower by a factor of 2 to 3.

[21] Daily mean AODs (at 670 nm) from Aerosol Robotic Network (AERONET) stations located in the INDOEX region are shown in Figure 5. Dharwar is a continental station on the west coast of India influenced by dust and anthropogenic aerosols from western India and west Asia whereas KCO is a remote station and is affected primarily by nearby sources of sea salt and long-range transport of aerosols. The model simulates the correct magnitude of AODs at Dharwar during January and February but the day-to-day variability is too weak and AODs are significantly underestimated in March. The situation is very similar at KCO, with an underestimation by a factor of 2 to 4 in March (Figure 5b). Some of the day-to-day variability may come from variability in the dust emissions which is not considered by the model. The reasons for the underestimation in March are discussed later in this section.

[22] AOD has also been estimated over the ocean from Meteosat-5 measurements by Leon *et al.* [2001]. The AOD (at 550 nm) is retrieved over the ocean outside of the sun glint area (white area in Figure 6) and has been validated in the northern Indian Ocean (NIO). In this comparison the model daily AODs are masked by the corresponding satellite retrievals so that monthly averages consist of the same measurement days in the model and the observation. The main features in the satellite retrievals are well reproduced by the model, with elevated values over the Arabian Sea and low values in the ITCZ. There is some disagreement between the satellite and model distributions near coastal regions, which is consistent with the comparisons made above. The rather large values over the SIO in the satellite observations are not found in the model. Contamination by

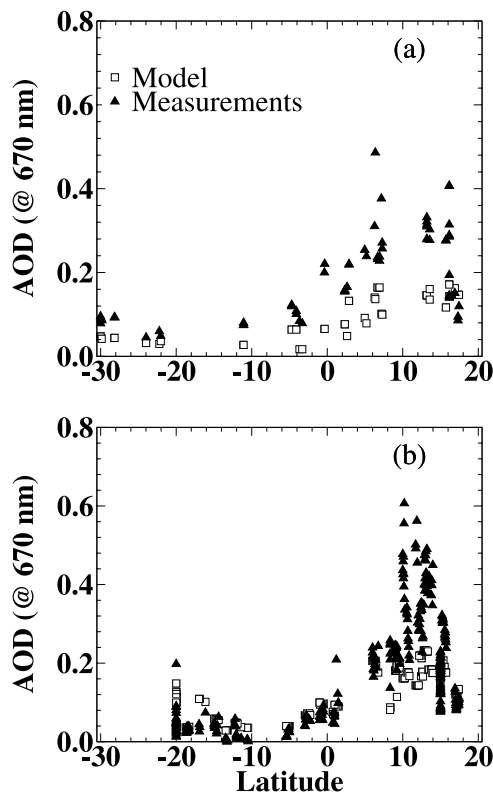


Figure 4. Modeled and measured AOD (at 670 nm) as a function of latitude for (a) the *Ronald Brown* and (b) the *Sagar Kanya* cruises. Measurements are from Quinn *et al.* [2002] and Jayaraman *et al.* [2001], respectively. Measurements are from handheld Microtops. The model results are sampled along the cruise track with a resolution of 6 hours.

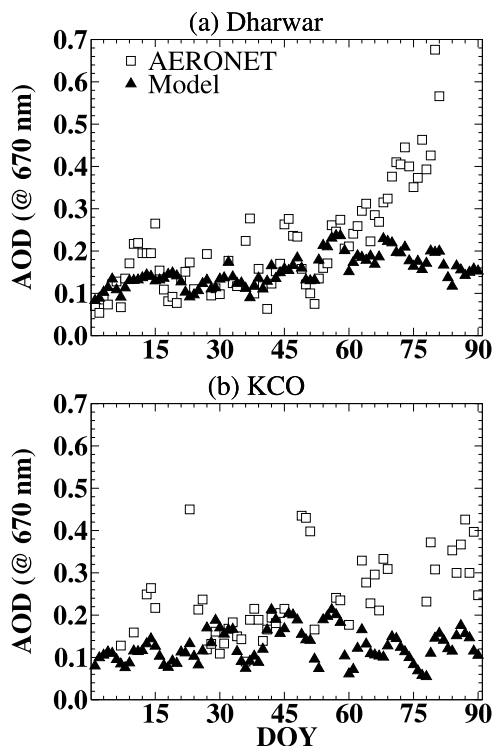


Figure 5. Measured (squares) and modeled (triangles) AOD (670 nm) at (a) Dharwar and (b) KCO for the period 1 January 1999 to 31 March 1999 (DOY ranging from 1 to 90).

broken clouds and the use of a single aerosol model in the retrieval algorithm (anthropogenic aerosols) leads to an overestimation of the AOD in the SIO.

[23] The model underestimation of aerosol surface concentrations and AOD at KCO particularly in March may stem from incorrect (i.e., too small) aerosol emissions, aerosol transport, and/or wet deposition. The year 1999 is characterized by a large number of fires over south and Southeast Asia as detected by the ATSR instrument. This larger than usual fire activity is accounted for in the model by increasing the open biomass-burning emissions in proportion to detected fire counts [Reddy and Boucher, 2004]. However, this does not result in a sufficient increase in AODs in March 1999. Furthermore emissions of carbonaceous aerosols from open biomass burning in the model are 2 to 3 times larger in March than in January and February over the INDOEX domain. Hence the underestimation of emissions may be not the sole reason for the too low AODs at KCO. The month of March is also characterized by low CO [Lobert and Harris, 2002] and large dust (Figure 3d) concentrations. An analysis of back trajectories conducted by Verver *et al.* [2001] showed that this period was associated with an increased flow from the west coast of India, more subject to dust emissions, and a decreased flow from the east coast of India, which is dominated by combustion aerosols. The aerosol Ångström coefficient (which is a measure of the aerosol size) measured at Dharwar was lower in March than in January and February, also suggesting a larger contribution of supermicron aerosols [Leon *et al.*, 2001]. Model winds are nudged to

ECMWF meteorological analyses, wherein the Indian Ocean region is characterized by a limited number of observations (in particular, there were no cloud motion winds assimilated during the period of INDOEX IFP), lowering the quality of ECMWF analyses [Bonazzola *et al.*, 2001]. Moreover, when compared to ECMWF precipitation fields, the model shows unrealistically high precipitation rates over the Arabian Sea and Bay of Bengal. This effect is more pronounced during the month of March, resulting in a too large scavenging of aerosols and a decrease in AOD at KCO. To examine further the role of wet deposition on the predicted aerosol concentrations and AOD, we carry out an experiment with wet deposition (in-cloud and below-cloud scavenging) set to zero over the entire INDOEX region (40° – 100° E, 30° S to 30° N). In this experiment (referred to as NOWETDEP), AODs are overestimated in January and February but still underestimated in March at Dharwar. The model therefore misses an aerosol source which most probably is supermicron dust, consistently with the analysis of Leon *et al.* [2001]. In NOWETDEP at KCO the agreement with observations is better, which points to wet deposition of aerosols over the ocean as one source of discrepancy.

4. Aerosol Distributions

[24] Distributions of average aerosol mass concentration at the surface are shown in Figure 7 for the period of January to March 1999. The largest sulfate concentrations are simulated over southwestern China and the east coast of India. There is a sulfate plume extending from south India to the Arabian Sea. Carbonaceous aerosols are mainly concentrated over the continent with largest values over Burma, northeast India, and southwestern China. There are large forest fires in these regions during the winter monsoon, resulting in significant emissions of carbonaceous aerosols which spread all over the Bay of Bengal with a plume extending to the Maldives. At about 10° S the aerosol plume encounters the ITCZ, where aerosols were either removed by wet deposition or transported vertically. We do not have emission maps for fly ash outside of India, which is the reason for the different pattern for this species. The largest fly ash concentrations are estimated over the intense source regions of the Indo-Gangetic valley and central India. The concentrations are significant and regional, if not global, estimates of fly ash emissions are highly desirable. Dust emissions occur over Arabia and west India and are transported into the Arabian Sea reaching the ITCZ. In the Southern Hemisphere dust from Australia spread over the SIO, which may not be realistic. The distribution of sea salt is quite different with a maximum in the SIO where strong surface winds are observed. On the Somalian coast the frequent occurrence of strong surface winds also results in a local maximum in sea salt concentrations. As expected there is an insignificant transport of sea salt into the Indian subcontinent during the winter monsoon.

[25] Aerosol vertical profiles over land and ocean are shown in Figure 8. Over the ocean sulfate, BC, OM, and fly ash concentrations slightly increase in the first 500 m and then decrease with height. Dust concentrations are largest at surface and decrease nearly exponentially with altitude whereas sea salt concentrations decrease more rapidly in

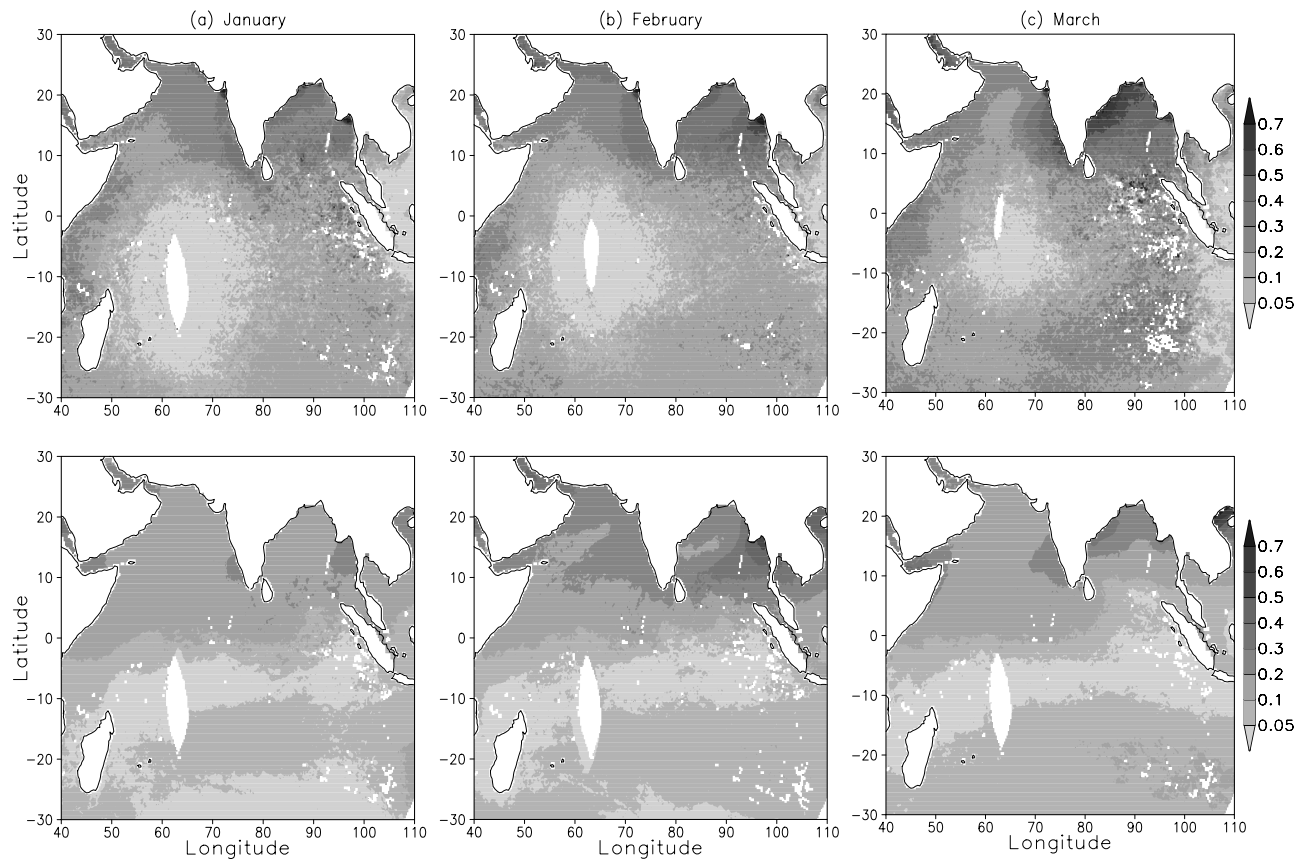


Figure 6. (a–c) Observed (from Meteosat, top panels) and modeled (bottom panels) monthly mean AOD at 550 nm during the three months of INDOEX-IFP99. The model values are masked with daily satellite retrievals before averaging. See color version of this figure in the HTML.

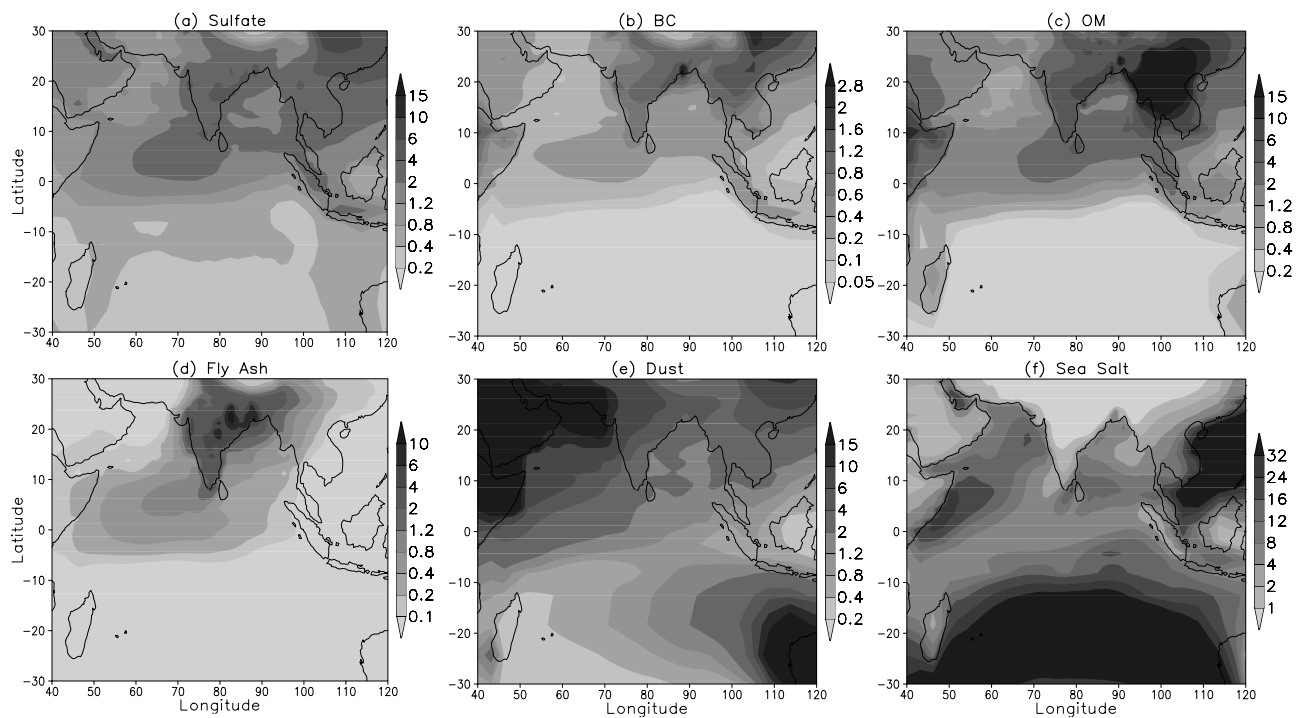


Figure 7. (a–f) Average simulated surface aerosol mass concentrations ($\mu\text{g m}^{-3}$) during IFP99. Fly ash emissions are only from India. See color version of this figure in the HTML.

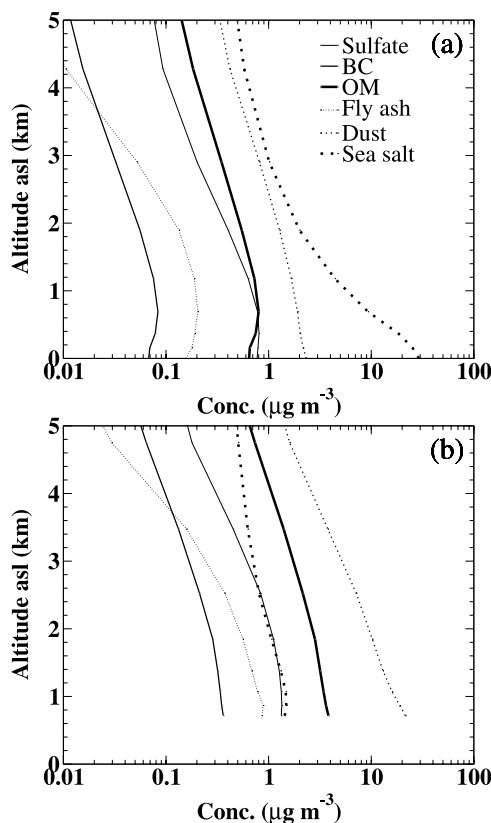


Figure 8. Vertical profiles of aerosol concentrations ($\mu\text{g m}^{-3}$) over the (a) oceanic and (b) land fractions of the INDOEX region (10°S to 30°N , 40°E to 100°E).

the first 2 km. Sedimentation, which applies for sea salt and dust, explains the different vertical profiles of these two aerosol types as compared to other types. There is more vertical mixing of aerosol concentrations over land (Figure 8b) because of a more turbulent boundary layer.

[26] There is also a clear contrast between the concentrations and burdens averaged over land and ocean. The land averaged burdens for BC, OM, fly ash, and dust are a factor of 2 to 5 larger than over the ocean (Table 1). The ratio of sulfate burdens averaged over land and ocean is lower at 1.5, which is due to the advection to the ocean of anthropogenic SO_2 prior to its oxidation to sulfate, a larger cloud cover over the ocean where oxidation of SO_2 can take place, and

Table 1. Aerosol Loads Over the INDOEX Region (10°S to 30°N , 40°E to 100°E) During the INDOEX-IFP99 Period^a

Parameter	Sulfate	BC	OM	Fly Ash	Dust	Sea Salt	Total
Surf. conc. entire region	0.89	0.13	1.32	0.31	6.39	37.31	
Surf. conc. ocean only	0.76	0.07	0.52	0.16	2.33	46.74	
Surf. conc. land only	1.33	0.36	3.82	0.86	21.49	2.39	
Burden entire region	1.08	0.52	5.53	0.91	15.91	41.29	
Burden ocean only	0.93	0.33	3.54	0.65	8.44	49.03	
Burden land only	1.57	1.23	11.50	1.96	43.65	12.54	
AOD entire region	0.027	0.005	0.025	0.0013	0.018	0.030	0.109
AOD ocean only	0.026	0.003	0.017	0.0009	0.011	0.036	0.097
AOD land only	0.028	0.015	0.059	0.0028	0.047	0.006	0.155

^aUnits for concentrations and burdens are $\mu\text{g m}^{-3}$ and mg m^{-2} , respectively. AODs given at 550 nm are dimensionless. Surf. conc., surface concentration.

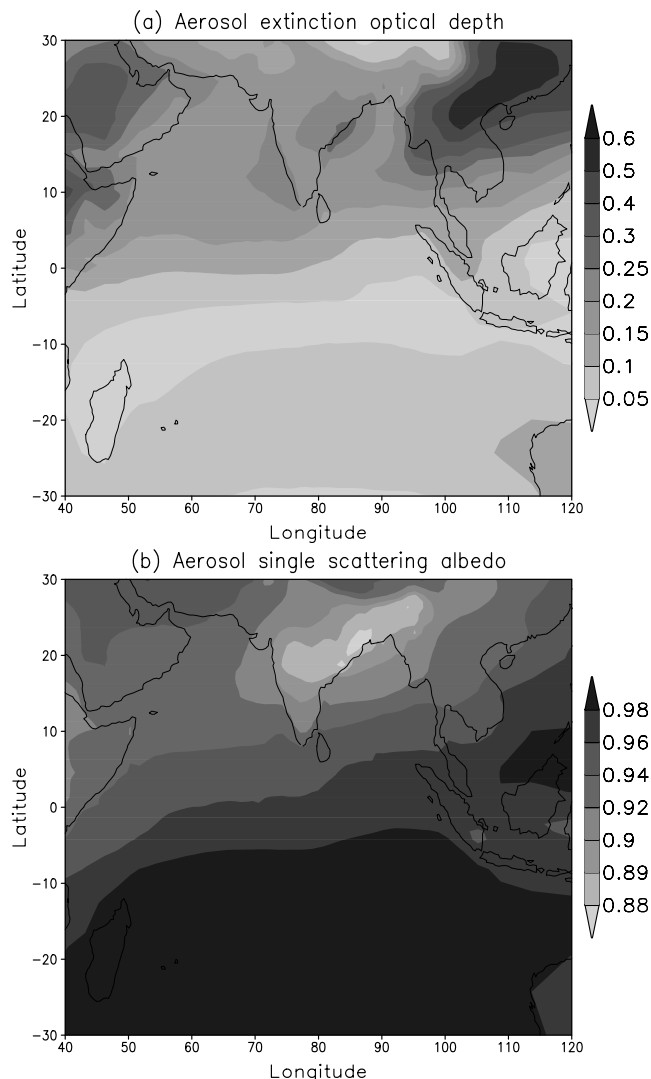


Figure 9. Average aerosol (a) extinction optical depth and (b) single-scattering albedo at 550 nm during IFP99. See color version of this figure in the HTML.

the existence of natural sources of sulfate over the ocean. Sea salt is emitted only over the oceans and as a result the burden of sea salt is a factor of 5 larger than over land.

5. Aerosol Optical Depth

[27] The average AOD (at 550 nm) distribution for the IFP99 period is shown in Figure 9a. There is a clear contrast in the AODs on each side of the ITCZ, with elevated values over the NIO (as large as 0.4) and smaller values over the SIO (smaller than 0.1). The ITCZ is located between 10° – 15°S and exhibits the smallest AODs at about 0.05. The largest AODs of the order of 0.5 are estimated over southwestern China where there are important sources of sulfur precursor gases and carbonaceous aerosols. AOD by sulfate peaks over southwestern China and the west coast of India (Figure 10a). Emissions in the Indo-Gangetic valley also result in AODs as large as 0.15 near Calcutta and over the Bay of Bengal. AOD by carbonaceous aerosols has the largest values over the continent. Large-scale forest fires

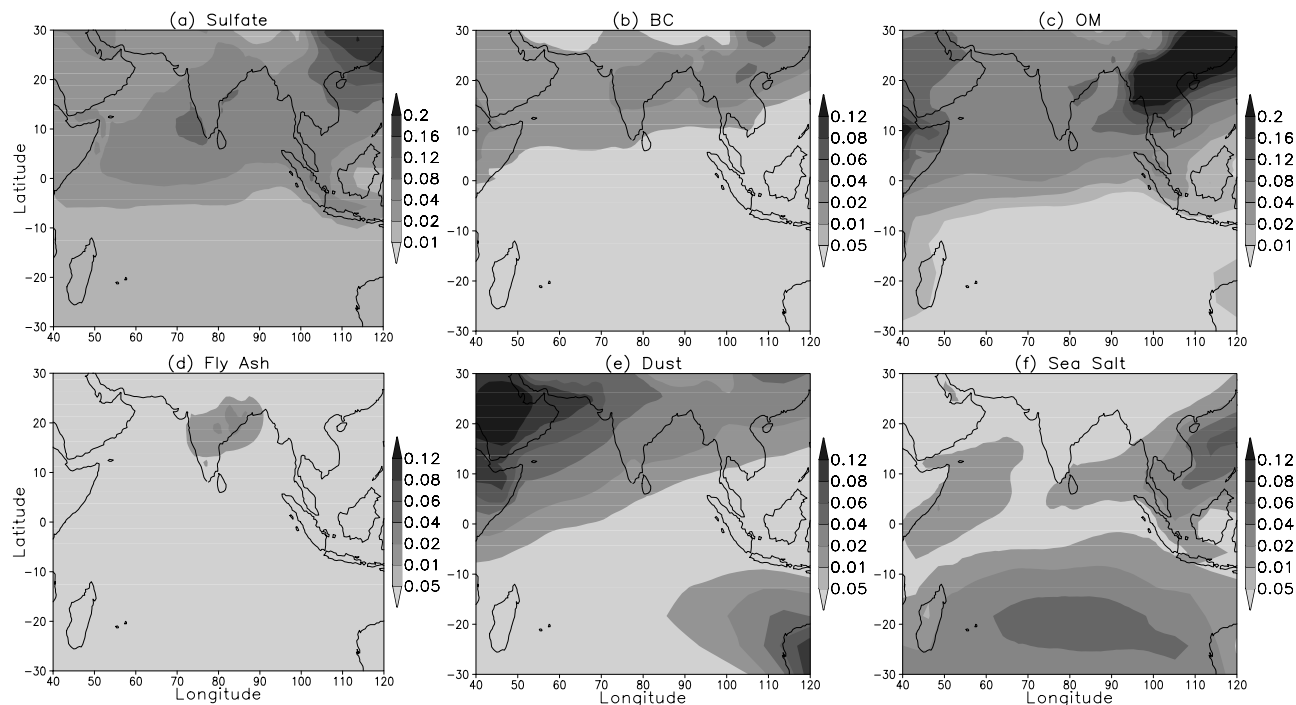


Figure 10. AOD at 550 nm from different aerosol species: (a) sulfate, (b) BC, (c) OM, (d) fly ash, (e) dust, and (f) sea salt. See color version of this figure in the HTML.

over Southeast Asia (Burma and Thailand) and northeast India result in AODs close to 0.3 (Figures 10b and 10c). Although BC emissions are only 9% of the total emissions of carbonaceous aerosols, the large mass extinction efficiency of BC compared to OM results in a contribution of about 20% to the AOD by carbonaceous aerosols. The land to ocean ratio in AOD is about 3, smaller than the corresponding ratio for burden, because of the larger RH over the ocean. The contribution of fly ash to the total AOD is not negligible over the source regions with values up to 10% (Figure 10d). Development of global, or at least regional, emission maps for this aerosol species is therefore very much needed. Dust is a significant contributor to the total AOD over the INDOEX region, especially over Arabia, west India, and Pakistan (Figure 10e). Dust contributes 30–40% to the total AOD over these regions. As expected AOD by sea salt dominates over the SIO, with significant contributions as well off the Somalian coast and over the Bay of Bengal (Figure 10f).

[28] Absorption of solar radiation by aerosols is mostly due to BC, with a mass absorption efficiency of $7.5 \text{ m}^2 \text{ g}^{-1}$ at 550 nm. Dust has a mass absorption efficiency of 1.29 and $0.36 \text{ m}^2 \text{ g}^{-1}$ for submicron and supermicron size ranges, respectively. BC contributes to about 80% and 90% of absorption AOD (at 550 nm) over the oceans and continent, respectively, with remaining portion accounted by OM and mineral dust. The key parameter to understand aerosol absorption is the aerosol single-scattering albedo (SSA), $\omega = \alpha_s / (\alpha_s + \alpha_a)$, where α_s and α_a are the mass scattering and absorption efficiencies, respectively. A comparison of model-simulated SSA (at 670 nm) and AERONET measurements for Goa and KCO is given in Table 2. The average SSA for the entire period at Goa is 0.92 ± 0.01 and agrees well with the measured value of 0.93 ± 0.02 . The average SSA

from the model at KCO is 0.95 ± 0.01 and is larger than the measured value of 0.92 ± 0.01 . The agreement in aerosol SSA at Goa indicate that the presence of absorbing (i.e., BC) and scattering aerosols (i.e., sulfate, OM, sea salt) are in the right proportion. The overestimation of the aerosol SSA at KCO, a remote station, may result from an overestimation of the sinks of absorbing aerosols as they are transported away from the sources or from a change in the aerosol mixture not accounted for in the model. The extinction coefficient of sulfate and OM increases as they are transported to KCO because of increasing RH, while BC keeps the same mass extinction coefficient. The assumption of external mixture differs from the actual state of aerosols in the atmosphere and contributes to some of the discrepancy in comparison between modeled and measured aerosol SSA. Predicted SSAs are of the order of 0.88–0.90 and 0.90–0.94 over the Bay of Bengal and the west coast of India, respectively. A quantitative assessment of the contributions of biomass and fossil fuel sources to atmospheric absorption by aerosols over the Indian Ocean is the subject of a future study.

6. Doubling of Asian BC Emissions

[29] *Dickerson et al.* [2002] measured carbon monoxide (CO) and BC on various platforms during IFP99 and

Table 2. Average Aerosol Single-Scattering Albedo at KCO and Goa During IFP99

	KCO	Goa
AERONET	0.92 ± 0.03	0.93 ± 0.02
Model (CONTROL exp.) ^a	0.95 ± 0.01	0.92 ± 0.01
Model (2xBC exp.) ^a	0.91 ± 0.02	0.87 ± 0.01

^aIn the model, aerosol SSAs were averaged only for days for which AERONET retrievals are available. Exp., experiment.

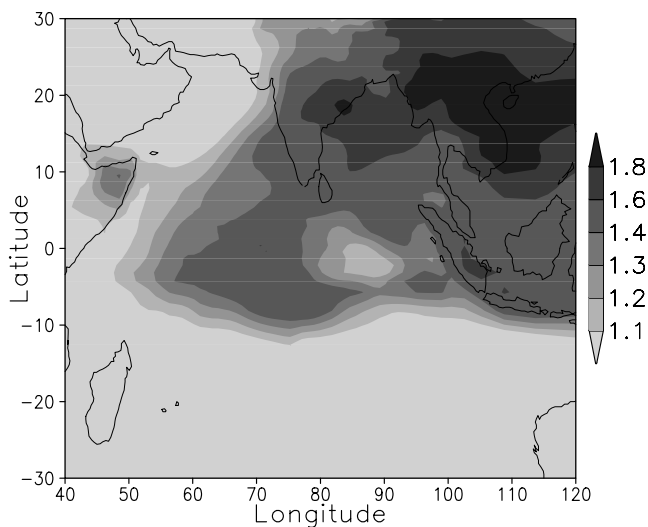


Figure 11. Ratio of the aerosol absorption optical depth at 550 nm from 2xBC to that from CONTROL. See color version of this figure in the HTML.

found that both concentrations correlate with an average slope in the range of 12.5×10^{-3} to 27×10^{-3} . Using this ratio of BC to CO concentrations and known CO emission strengths, they estimate a lower limit of 1.0 and a probable range of 2–3 Tg yr⁻¹ for BC emissions from south Asia. In contrast bottom-up emission inventories which are used in this study place BC emissions from south Asia at about 0.6 Tg yr⁻¹. To understand whether BC emissions are really underestimated over Asia in current emission inventories, we carry out an experiment in which BC emissions from Asia are doubled. This experiment is referred to as 2xBC whereas the experiment described in the previous sections is simply labeled as CONTROL.

[30] BC emissions from south Asia in the CONTROL and 2xBC experiments are 0.55 and 1.1 Tg yr⁻¹, respectively. In the 2xBC experiment, predicted surface concentrations at KCO are about twice that of the CONTROL experiment, which results in a somewhat better agreement with the observations. Despite this increase in concentrations, the large values measured on 14–18 February are not reproduced by the model. With the increase in BC emissions, the simulated aerosol SSA at KCO agrees better with measurements but a discrepancy arises for the simulated aerosol SSA at Goa (Table 2). This demonstrates that absorbing aerosols (e.g., BC) in the CONTROL run are not necessarily underrepresented in proportion to scattering aerosols (e.g., sulfate and OM). Other uncertainties, such as those associated with BC and OM optical properties and hygroscopicity, prevent us from definite conclusion of BC emission strength. Doubling of the BC emissions in Asia results in an increase in AOD (at 550 nm) of 10% and 5% over land and ocean, respectively. Over the Indian subcontinent and Southeast Asia aerosol absorption optical depth is primarily contributed by BC and it increases by a factor of 1.5 to 2 in the 2xBC experiment (Figure 11). The increase is about 50% over the NIO to the ITCZ (which is roughly at 10°S). The implications of increased BC emissions for

atmospheric absorption of solar radiation are discussed in section 8.

7. Contribution of South Asia

[31] Lagrangian back trajectory analysis of air parcels done for IFP99 suggested that aerosols observed over the Indian Ocean were advected primarily from south Asia with contributions from east and Southeast Asia, Africa, and Arabia [Verver *et al.*, 2001; Franke *et al.*, 2003]. However, Lagrangian back trajectories do not represent mixing processes in the atmosphere and may underestimate the variability in atmospheric transport. Therefore Eulerian approaches are also needed, either in forward mode if one is interested in the fate of pollutants emitted in a given region, or in backward mode if one is interested in the origin of pollutants observed at a given site or region (F. Hourdin *et al.*, Eulerian backtracking of atmospheric tracers: Adjoint derivation, parametrization of subgrid-scale transport and numerical aspects, submitted to *Quarterly Journal of the Royal Meteorological Society*, 2003). We therefore carry out one further simulation with emissions only from south Asian countries (experiment labeled SASIA). These countries are member countries of the South Asian Association for Regional Cooperation (SAARC), namely Bangladesh, Bhutan, India, Maldives, Nepal, Pakistan, and Sri Lanka (Figure 12). The comparison of the CONTROL and SASIA experiments provides the contribution of the SAARC region to aerosol concentrations and optical depth over the INDOEX domain.

[32] The contribution of south Asia to estimated aerosol surface concentrations is shown in Figure 13 for the period January to March 1999. Emissions from south Asia are preferentially transported into the Indian Ocean. Over the Indian subcontinent local and regional sources account for a large fraction of the estimated sulfate (80–90%). The

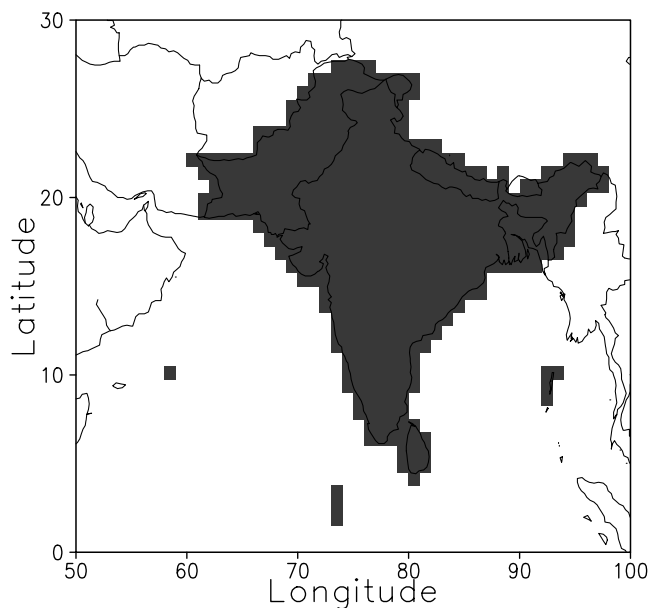


Figure 12. Map of the SAARC region which includes Bangladesh, Bhutan, India, Maldives, Nepal, Pakistan, and Sri Lanka.

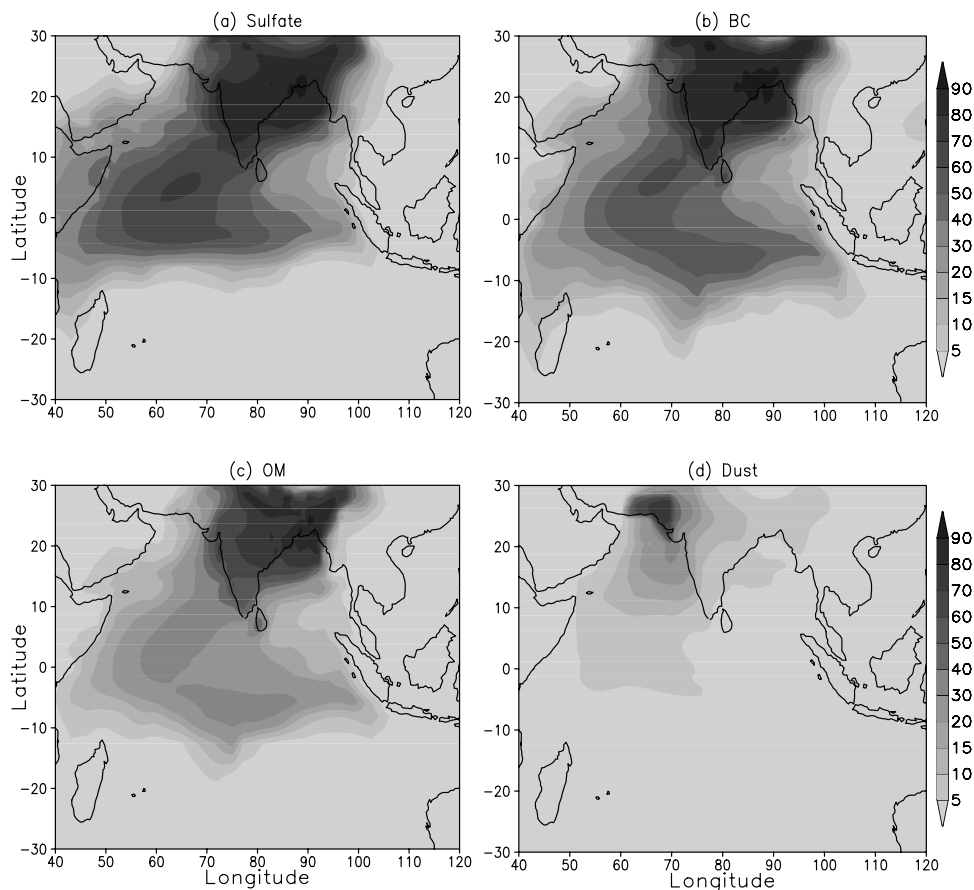


Figure 13. Contribution (%) of the SAARC region to aerosol surface concentrations: (a) sulfate, (b) BC, (c) OM, and (d) dust. See color version of this figure in the HTML.

sulfate over the NIO is predominantly from south Asian sources with a contribution of 40–70%. Prevailing dry conditions during this season result in transport of continental sulfur as far as 10°S where the contribution amounts to 5–20%. Carbonaceous aerosols (BC + OM) from south Asia are mostly concentrated over the continent and account for up to 80% of surface concentrations. Over the Indian Ocean, south Asian sources account for less than 50% of surface concentrations, with the exception of the Bay of Bengal where the contribution can reach 80% up to 400 km offshore of Calcutta. In the Indo-Gangetic valley the use of biofuels, particularly dung-cake and coal in brick kilns, generates considerable amount of OM [Reddy and Venkataraman, 2002a, 2002b; Habib *et al.*, 2004] which is transported into the Bay of Bengal. South Asian dust emission sources are small compared to other sources over Arabia and west Asia and account for less than 10% of estimated dust surface concentrations over most of the Indian Ocean.

[33] The frequent occurrence of high-altitude aerosol plumes over the INDOEX region is well documented from lidar profiles and aircraft measurement [Ramanathan *et al.*, 2001; Müller *et al.*, 2001]. Elevated aerosol plumes may be transported over large distances so the contribution of emissions from a given region may be different for surface or column concentrations. This is illustrated in Figure 14, which shows the contribution of south Asia to AOD by

species for the IFP99 period. Similar to the surface concentrations AOD by sulfate over the region is dominated by the south Asian sources. Over most of the study region the contribution is in the range of 60 to 70%, signifying that south Asia is the primary source of sulfate observed over the NIO. In contrast, the contribution of south Asia to AOD by carbonaceous aerosols does not exceed 50%, even over the continent. The contribution to AOD is therefore smaller than to surface concentrations, which can be explained by long-range transport in the free troposphere from farther regions. The low contribution of south Asia to AOD by carbonaceous aerosols is due to transport of biomass-burning emissions from Africa [de Laat *et al.*, 2001]. As south Asia is not a major source of dust emissions, its contribution to AOD by dust is smaller than 10% over the Arabian Sea and 20% over Pakistan and western India. Over the NIO emissions from south Asia contribute 50% to the total AOD (at 550 nm). At KCO, south Asian emissions account for 45% of the AOD during the entire IFP99 period, with contributions of 70% for sulfate, 46% for BC, 31% for OM, and 4% for dust. With geographically tagged radon emissions, Rasch *et al.* [2001] estimated the contribution of different regions to predicted radon concentrations at the surface and 2.5 km altitude. The contribution of radon emitted from the Indian subcontinent to surface concentrations was larger than the contribution at 2.5 km. However, the contribution of radon emitted over Africa was smaller at

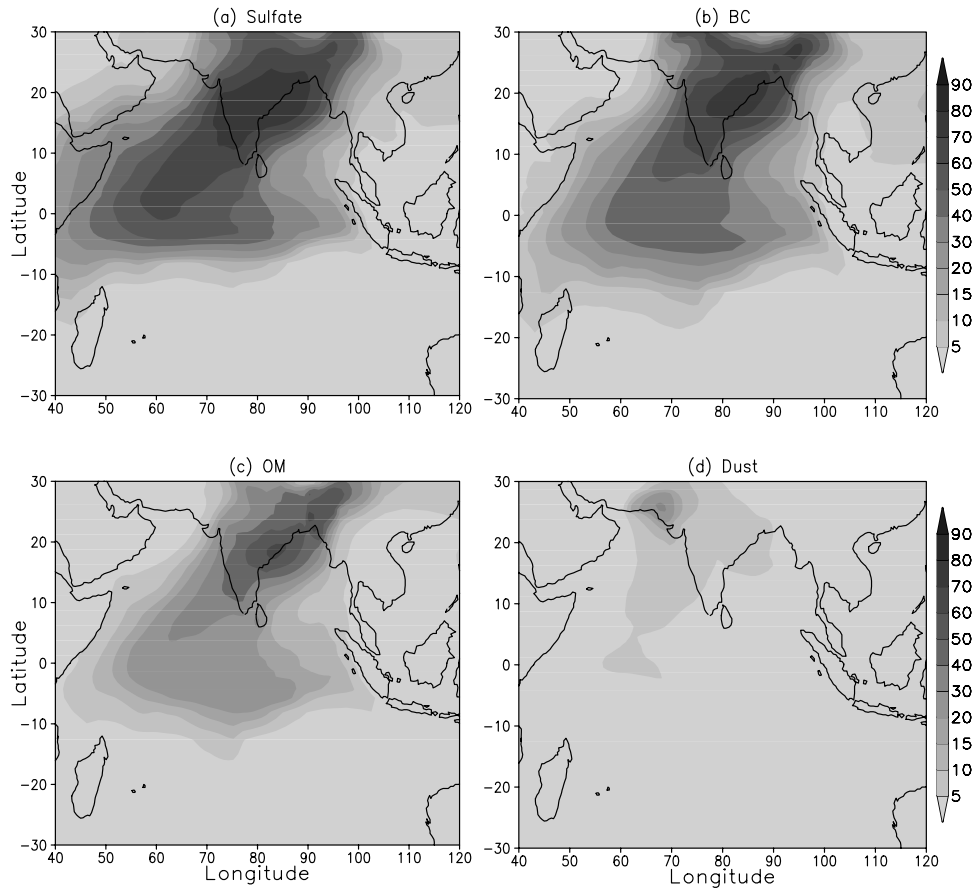


Figure 14. Same as Figure 13 but for AOD. See color version of this figure in the HTML.

the surface than at 2.5 km altitude by a factor of 2 to 4. This corroborates the role of elevated plumes from biomass burning in Africa to AOD over the Indian Ocean.

8. Radiative Forcing Estimates

[34] One of the primary objectives of the INDOEX experiment was to determine the aerosol direct radiative forcing due to anthropogenic aerosols. Assuming aerosols are present as an external mixture we estimate the aerosol direct radiative forcing in clear- and all-sky conditions. In this study, we do not consider aerosol radiative effects in the longwave, although longwave aerosol forcing can be significant in regions with large dust loadings [Lubin *et al.*, 2002]. The aerosol forcing efficiency can be defined as the radiative forcing per AOD unit (at 550 nm). The average clear-sky forcing efficiencies estimated at KCO at top of the atmosphere (f_e^{toa}) and surface (f_e^{surf}) are -19 and -49 W m^{-2} , respectively. Using NASA CERES Earth radiation budget measurements, Sathesh and Ramanathan [2000] estimated f_e^{toa} and f_e^{surf} at KCO at -25 and -70 to -75 W m^{-2} , respectively. In their GCM, Collins *et al.* [2002] calculate f_e^{toa} and f_e^{surf} as -22 and -73 W m^{-2} , respectively. Our forcing efficiencies are comparable with measurements and previous model estimates for IFP99, but with lower values for f_e^{surf} , which again indicates an underestimation of aerosol absorption. The average aerosol shortwave direct clear-sky radiative forcing is shown in

Figure 15 at TOA (F_{toa}), surface (F_{surf}), and within the atmosphere ($F_{\text{atm}} = F_{\text{toa}} - F_{\text{surf}}$). For the sake of comparison we also present on the right panels estimates over the ocean made from the Polarization and Directionality of the Earth's Reflectances (POLDER-1) satellite and AERONET observations. These estimates are averaged values for the period January to March 1997 from Bellouin *et al.* [2003]. The radiative forcing at TOA is negative over most of the region, with some patches of positive values over regions with bright surfaces (desert and Himalayas). The SIO experiences a radiative forcing of about -2 W m^{-2} primarily from sea salt and sulfate aerosols. In contrast the NIO and continents are characterized by values as low as -8 W m^{-2} . Aerosols over the SIO exhibit little absorption and F_{surf} is only slightly larger in magnitude than F_{toa} . Over the SIO, F_{atm} is smaller than $+5$ W m^{-2} whereas over the NIO and continents F_{atm} exhibit values up to $+25$ W m^{-2} with enhanced values over northeast India, Southeast Asia, and southwestern China. Over Arabia the presence of dust and bright desert surfaces also results in F_{atm} larger than $+20$ W m^{-2} . The ratio between F_{surf} and F_{toa} ranges from 2 to 4 over the NIO, with larger values near the coastal regions, which compares well with estimates made by Tahnk and Coakley [2002] and Bellouin *et al.* [2003].

[35] In the 2xBC experiment (Figure 15, middle panels) F_{toa} over the ocean does not change significantly because of the rather low surface albedo. However, F_{toa} turns positive over many parts of the Indian subcontinent because of

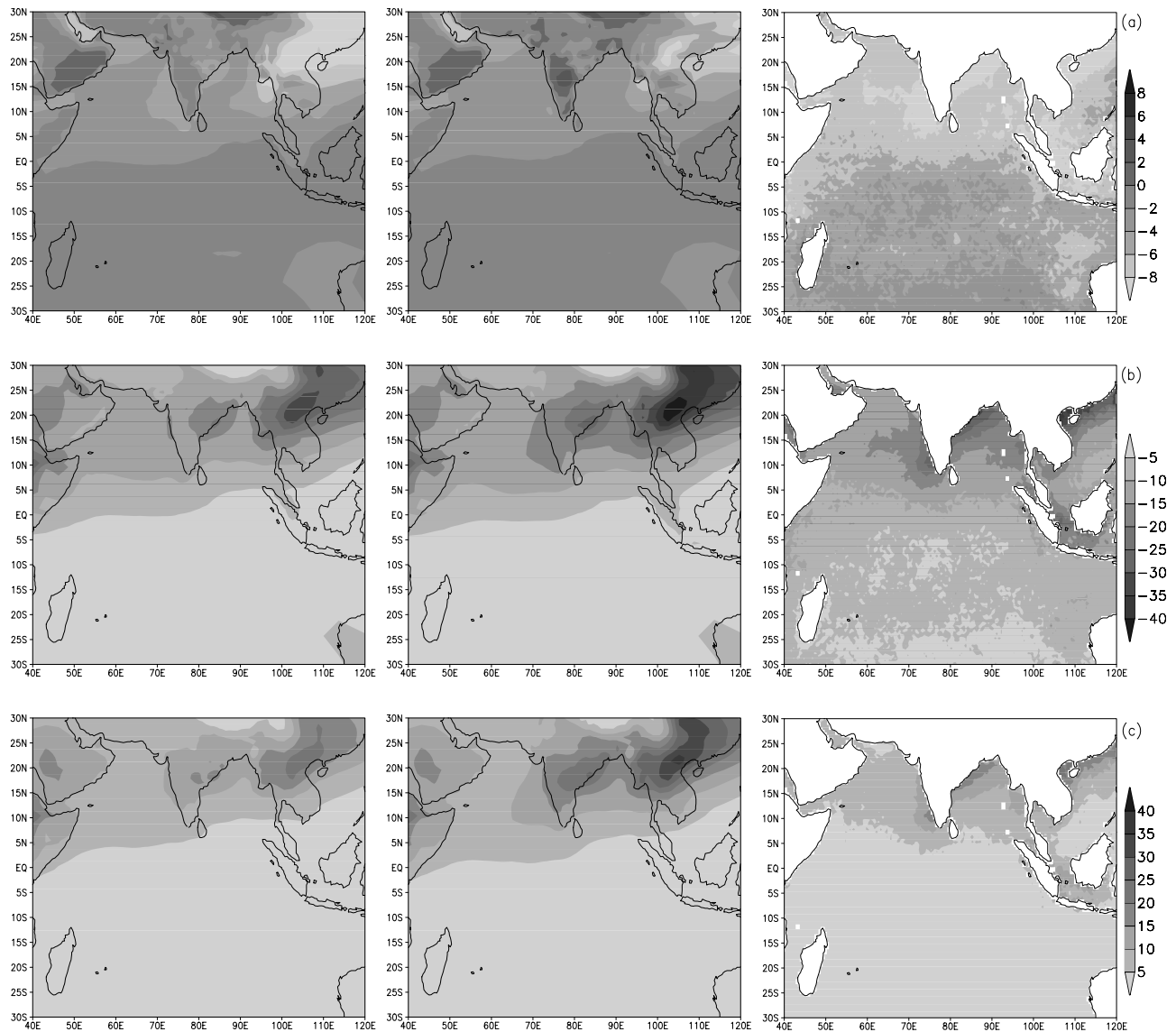


Figure 15. January to March averaged aerosol shortwave direct clear-sky radiative forcing (W m^{-2}) over the INDOEX region: (a) top of the atmosphere, (b) surface, and (c) in the atmosphere. Left and middle panels are for the CONTROL and 2xBC experiments for 1999, respectively, while the right panels depict POLDER estimates for 1997 from *Bellouin et al.* [2003]. See color version of this figure in the HTML.

increased concentrations of atmospheric BC. Over southwestern China the presence of large amounts of sulfate aerosol cancels out the positive forcing induced by the increased atmospheric BC concentrations and F_{toa} remains negative. In the 2xBC experiment, increased BC emissions enhance F_{surf} by a factor of 1.4 over northeast India, Burma, and southwestern China. Over the NIO, F_{surf} increases by a factor of 1.1–1.3 with larger values over the Bay of Bengal. Finally, F_{atm} increases by a factor of 1.6 over northeast India, 1.5 over China, and 1.2–1.4 over the NIO.

9. Conclusions

[36] The fate of atmospheric aerosols has been simulated along with their direct radiative effects for the INDOEX Intensive Field Phase during January to March 1999. We

used the LMDZT GCM with a zoom over the INDOEX domain and surface winds nudged to ECMWF analysis fields. High-resolution aerosol emissions for India and Asia have been nested into global emission maps. The seasonal variability in open biomass-burning emissions have been inferred from satellite detected fire counts. The performance of the model has been evaluated by a comparison with in situ measurements from ships, ground-based stations, and satellites. The model reproduces the north-to-south spatial gradient in aerosol mass concentrations and optical depth. However, the model cannot reproduce the large concentrations observed during some episodes, especially in the month of March 1999. Although the observed increase in fire activity over Southeast Asia during March 1999 has been accounted for in the model by scaling the open biomass-burning emissions with measured fire counts,

emissions in the model may still be underestimated. It should also be noted that there was at the time of INDOEX a general lack of meteorological observations over the Indian Ocean, which lowers the quality of ECMWF analyses [Bonazzola *et al.*, 2001]. The distributions of aerosol concentrations show the largest concentrations over southwestern China with a plume extending into the Bay of Bengal and traveling over to the Maldives. Indian emissions result in regional maxima over Calcutta and Bombay. There are two preferential outflow channels from India one extending from Bombay transporting aerosols into the Arabian Sea and a second one extending from Calcutta transporting aerosols from the Indo-Gangetic region into the Bay of Bengal.

[37] The contribution of carbonaceous aerosols to the total AOD is 50–60% over Southeast Asia and northeast India and 40% over the Indian Ocean. BC accounts for 20–25% of the AOD by carbonaceous aerosols and for 10% of the total AOD at 550 nm. Sulfate is the second largest contributor to the estimated AOD. In contrast to carbonaceous aerosols the contribution of sulfate is larger over the ocean (30–50%) than over land (15–30%). This is because of the advection of anthropogenic SO₂, natural sources of sulfate precursors, the presence of clouds which facilitate the oxidation of SO₂, and a larger RH growth factor over the ocean. The contribution of fly ash to the estimated AOD can be as large as 10% over the source regions, which argues for the development of regional emission inventories for this aerosol species. Dust dominates over the Arabian Sea and western Asia with contributions of 30–50% to the total AOD. Sea salt is concentrated over the SIO and accounts for most of the AOD there, while over the NIO its contribution is typically smaller than 10%.

[38] Aerosol single-scattering albedo estimated is within ± 0.03 that of measured values at Goa and KCO. The observed radiative forcing efficiency is well reproduced by the model at TOA but is somewhat underestimated at the surface. During the northeast winter monsoon, natural and anthropogenic aerosols reduce the solar flux reaching the surface by 20–30 W m⁻² with atmospheric absorption of solar radiation by aerosols of 25 W m⁻². This leads to a decrease of 10–15% in insolation at the surface in clear sky conditions. The impact of a reduction in insolation at the surface on the regional climate is the subject of active research.

[39] We examined the impact of a doubling of Asian BC emissions on aerosol radiative effects. A doubling of Asian BC emissions results in an increase of 40–80% in the aerosol absorption optical depth over the region and a decrease of aerosol SSA by 5–10%. The predicted aerosol SSA in this case is lower than measured at Goa and KCO. This suggests that BC emissions are not underestimated in proportion to other (scattering) aerosols species in the standard model setup. Atmospheric forcing by aerosols increase by 60% over the continent and 20–40% over the NIO in the 2xBC experiment.

[40] The contribution of south Asia to the aerosol concentrations and optical depth over the Indian Ocean has been quantified. South Asia is the dominant source of sulfate aerosols over the INDOEX domain. Sources from south Asia account for less than 50% of total carbonaceous aerosols over the entire Indian Ocean. The presence of

aerosol plumes generated over surrounding regions of Africa and Southeast and east Asia into the Indian Ocean lowers the contribution from south Asia.

[41] While the INDOEX field campaign has helped answering a number of questions, there are new issues which have been raised and need to be addressed in future studies. We need to reconcile the large observed aerosol concentrations with present emission inventories, especially for carbonaceous aerosols. It is not clear either what are the relative strengths of emissions from fossil fuel and biomass burning. Multiyear GCM simulations are also needed to understand the winter and summer monsoon variability in aerosol concentrations. Our research will further focus on aerosol source attribution, understanding of the atmospheric and oceanic response to the radiative forcings by atmospheric aerosols during the winter and summer Indian monsoons.

[42] **Acknowledgments.** We would like to thank two anonymous reviewers for their thorough reading of the manuscript and constructive comments. This work was supported by the Indo-French Centre for the Promotion of Advanced Research (IFCPAR) and Environment and Climate Programme of the European Community (PHOENICS contract EVK2-CT-2001-00098). Computing time was provided by CNRS/IDRIS under projects 021167 and 031167. The Laboratoire d'Optique Atmosphérique is an institute of the "Fédération de Recherche" FR1818 of the CNRS. We thank P. Quinn for providing aerosol measurements made onboard the *Ronald Brown* and Z. Chowdhury for providing aerosol measurements made at KCO. S. Verma's visit to LOA (France) was supported by START.

References

- Bellouin, N., O. Boucher, D. Tanré, and O. Dubovik (2003), Aerosol absorption over the clear-sky oceans deduced from POLDER-1 and AERONET observations, *Geophys. Res. Lett.*, *30*(14), 1748, doi:10.1029/2003GL017121.
- Bonazzola, M., L. Picon, H. Laurent, F. Hourdin, G. Sèze, H. Pawlowska, and R. Sadourny (2001), Retrieval of large-scale wind divergences from infrared Meteosat-5 brightness temperatures over the Indian Ocean, *J. Geophys. Res.*, *106*, 28,113–28,128.
- Boucher, O., and M. Pham (2002), History of sulfate aerosol radiative forcings, *Geophys. Res. Lett.*, *29*(9), 1308, doi:10.1029/2001GL014048.
- Boucher, O., M. Pham, and C. Venkataraman (2002), Simulation of the atmospheric sulfur cycle in the Laboratoire de Météorologie Dynamique general circulation model: Model description, model evaluation, and global and European budgets, *Note Sci. de l'IPSL* *23*, 27 pp., Inst. Pierre-Simon Laplace, Paris.
- Chowdhury, Z., L. S. Hughes, L. G. Salmon, and G. R. Cass (2001), Atmospheric particle size and composition measurements to support light extinction calculations over the Indian Ocean, *J. Geophys. Res.*, *106*, 28,597–28,605.
- Collins, W. D., P. J. Rasch, B. E. Eaton, D. W. Fillmore, J. T. Kiehl, C. T. Beck, and C. S. Zender (2002), Simulation of aerosol distributions and radiative forcing for INDOEX: Regional climate impacts, *J. Geophys. Res.*, *107*(D19), 8028, doi:10.1029/2000JD000032.
- de Laat, A. T. J., J. A. de Gouw, and J. Lelieveld (2001), Model analysis of trace gases measurements and pollution impact during INDOEX, *J. Geophys. Res.*, *106*, 28,469–28,480.
- Dickerson, R. R., M. O. Andreae, T. Campos, O. L. Mayol-Bracero, C. Neusüß, and D. G. Streets (2002), Analysis of black carbon and carbon monoxide observed over the Indian Ocean: Implications for emissions and photochemistry, *J. Geophys. Res.*, *107*(D19), 8017, doi:10.1029/2001JD000501.
- Fouquart, Y., and B. Bonnel (1980), Computations of solar heating of the Earth's atmosphere: A new parameterization, *Beitr. Phys. Atmos.*, *53*, 35–63.
- Franke, K., A. Ansmann, D. Müller, D. Althausen, C. Venkataraman, M. S. Reddy, F. Wagner, and R. Scheele (2003), Optical properties of the Indo-Asian haze layer over the tropical Indian Ocean, *J. Geophys. Res.*, *108*(D2), 4059, doi: 10.1029/2002JD002473.
- Giorgi, F., and W. L. Chameides (1986), Rainout lifetimes of highly soluble aerosols and gases as inferred from simulations with a general circulation model, *J. Geophys. Res.*, *91*, 14,367–14,376.
- Guazzotti, S. A., et al. (2003), Characterization of pollution outflow from India and Arabia: Biomass burning and fossil fuel combustion, *J. Geophys. Res.*, *108*(D15), 4485, doi:10.1029/2002JD003277.

- Habib, G., C. Venkataraman, M. Shrivastava, R. Banerjee, and R. R. Dickerson (2004), New methodology for estimating biofuel consumption in India: Atmospheric emissions of black carbon and sulfur dioxide, *Global Biogeochem. Cycles*, *18*, GB3007, doi:10.1029/2003GB002157.
- Hauglustaine, D. A., F. Hourdin, L. Jourdain, M.-A. Filiberti, S. Walters, J.-F. Lamarque, and E. A. Holland (2004), Interactive chemistry in the Laboratoire de Météorologie Dynamique general circulation model: Description and background tropospheric chemistry evaluation, *J. Geophys. Res.*, *109*, D04314, doi:10.1029/2003JD003957.
- Hourdin, F., and A. Armand (1999), The use of finite-volume methods for atmospheric advection of trace species. Part I: Test of various formulations in a general circulation model, *Mon. Weather Rev.*, *127*, 822–837.
- Jayaraman, A., S. K. Satheesh, A. P. Mitra, and V. Ramanathan (2001), Latitude gradient in aerosol properties across the Inter Tropical Convergence Zone: Results from the joint Indo-US study onboard *Sagar Kanya*, *Curr. Sci.*, *80*, 128–137.
- Leon, J.-F., et al. (2001), Large scale advection of continental aerosols during INDOEX, *J. Geophys. Res.*, *106*, 28,427–28,440.
- Lobert, J. M., and J. M. Harris (2002), Trace gases and air mass origin at Kaashidhoo, Indian Ocean, *J. Geophys. Res.*, *107*(D19), 8013, doi:10.1029/2001JD000731.
- Lubin, D., S. K. Satheesh, G. McFarquar, and A. J. Heymsfield (2002), Longwave radiative forcing of Indian Ocean tropospheric aerosol, *J. Geophys. Res.*, *107*(D19), 8004, doi:10.1029/2001JD001183.
- Mayol-Bracero, O. L., R. Gabriel, M. O. Andreae, T. W. Kirchstetter, T. Novakov, J. Ogren, P. Sheridan, and D. G. Streets (2002), Carbonaceous aerosols over the Indian Ocean during the Indian Ocean Experiment (INDOEX): Chemical characterization, optical properties, and probable sources, *J. Geophys. Res.*, *107*(D19), 8030, doi:10.1029/2000JD000039.
- Minvielle, F., et al. (2004a), Modeling of the transport of aerosols during INDOEX 1999 and comparison with experimental data, Part 1: Carbonaceous aerosol distribution, *Atmos. Environ.*, *38*, 1811–1822.
- Minvielle, F., et al. (2004b), Modeling of the transport of aerosols during INDOEX 1999 and comparison with experimental data, Part 2: Continental aerosol and their optical depth, *Atmos. Environ.*, *38*, 1823–1837.
- Monahan, E. C., D. E. Spiel, and K. L. Davidson (1986), A model of marine aerosol generation via whitecaps and wave disruption, in *Oceanic Whitecaps and Their Role in Air-Sea Exchange Processes*, edited by E. C. Monahan and G. M. Niocaill, pp. 167–174, D. Reidel, Norwell, Mass.
- Morcrette, J.-J. (1991), Radiation and cloud radiative properties in the European Centre for Medium Range Weather Forecasts forecasting systems, *J. Geophys. Res.*, *96*, 9121–9132.
- Müller, D., K. Franke, F. Wagner, D. Althausen, A. Ansmann, J. Heintzenberg, and G. H. L. Verver (2001), Vertical profiling of optical and physical particle properties over the tropical Indian Ocean with six-wavelength lidar, Part II, Case studies, *J. Geophys. Res.*, *106*, 28,577–28,596.
- Neusüß, C., T. Gnauk, A. Plewka, H. Herrmann, and P. K. Quinn (2002), Carbonaceous aerosol over the Indian Ocean: OC/EC fractions and selected specifications from size-segregated onboard samples, *J. Geophys. Res.*, *107*(D19), 8031, doi:10.1029/2001JD000327.
- Novakov, T., M. O. Andreae, R. Gabriel, T. W. Kirchstetter, O. L. Mayol-Bracero, and V. Ramanathan (2000), Origin of carbonaceous aerosols over the tropical Indian Ocean: Biomass burning or fossil fuels?, *Geophys. Res. Lett.*, *27*, 4061–4064.
- O'Dowd, C. D., B. Davison, J. A. Lowe, M. H. Smith, R. M. Harrison, and C. N. Hewitt (1997), Biogenic sulphur emissions and inferred sulphate CCN concentrations in and around Antarctica, *J. Geophys. Res.*, *102*, 12,839–12,854.
- Olivier, J. G. J., and J. J. M. Berdowski (2001), Global emissions sources and sinks, in *The Climate System*, edited by J. Berdowski, R. Guicherit, and B. J. Heij, pp. 33–78, A. A. Balkema, Brookfield, Vt.
- Quinn, P. K., D. J. Coffman, T. S. Bates, T. L. Miller, J. E. Johnson, E. J. Welton, C. Neusüß, M. Miller, and P. J. Sheridan (2002), Aerosol optical properties during INDOEX 1999: Means, variability, and controlling factors, *J. Geophys. Res.*, *107*(D19), 8020, doi:10.1029/2000JD000037.
- Ramanathan, V., et al. (2001), Indian Ocean Experiment: An integrated analysis of the climate forcing and effects of the great Indo-Asian haze, *J. Geophys. Res.*, *106*, 28,371–28,398.
- Rasch, P. J., W. D. Collins, and B. E. Eaton (2001), Understanding the Indian Ocean Experiment (INDOEX) aerosol distributions with an aerosol assimilation, *J. Geophys. Res.*, *106*, 7337–7355.
- Reddy, M. S., and O. Boucher (2004), A study of the global cycle of carbonaceous aerosols in the LMDZT general circulation model, *J. Geophys. Res.*, *109*, D14202, doi:10.1029/2003JD004048.
- Reddy, M. S., and C. Venkataraman (2002a), Inventory of aerosol and sulfur dioxide emissions from India: I. Fossil fuels combustion, *Atmos. Environ.*, *36*, 677–697.
- Reddy, M. S., and C. Venkataraman (2002b), Inventory of aerosol and sulfur dioxide emissions from India: II. Biomass combustion, *Atmos. Environ.*, *36*, 677–697.
- Reddy, M. S., O. Boucher, and C. Venkataraman (2002), Seasonal carbonaceous aerosol emissions from open biomass burning in India, *Bull. Indian Aerosol Sci. Technol. Assoc.*, *14*, 239–243.
- Russell, P. B., P. V. Hobbs, and L. L. Stowe (1999), Aerosol properties and radiative effects in the United States east coast haze plume: An overview of the Tropospheric Aerosol Radiative Forcing Observational Experiment (TARFOX), *J. Geophys. Res.*, *104*, 2213–2222.
- Satheesh, S. K., and V. Ramanathan (2000), Large differences in tropical aerosol forcing at the top of the atmosphere and Earth's surface, *Nature*, *405*, 60–63.
- Satheesh, S. K., and J. Srinivasan (2002), Enhanced aerosol loading over Arabian Sea during pre-monsoon season: Natural or anthropogenic?, *Geophys. Res. Lett.*, *29*(18), 1874, doi:10.1029/2002GL015687.
- Streets, D. G., et al. (2003), An inventory of gaseous and primary aerosol emissions in Asia in the year 2000, *J. Geophys. Res.*, *108*(D21), 8809, doi:10.1029/2002JD003093.
- Tahnk, W. R., and J. A. Coakley Jr. (2002), Aerosol optical depths and direct radiative forcing for INDOEX derived from AVHRR: Observations, January–March 1996–2000, *J. Geophys. Res.*, *107*(D19), 8010, doi:10.1029/2000JD000183.
- Tegen, I., and I. Fung (1995), Contribution to the atmospheric mineral aerosol load from land surface modification, *J. Geophys. Res.*, *100*, 18,707–18,726.
- Tiedtke, M. (1989), A comprehensive mass flux scheme for cumulus parameterization in large-scale models, *Q. J. R. Meteorol. Soc.*, *117*, 1779–1800.
- Turpin, B. J., and H.-J. Lim (2001), Species contributions to PM_{2.5} mass concentrations: Revisiting common assumptions for estimating organic mass, *Aerosol Sci. Technol.*, *35*, 602–610.
- van Leer, B. (1977), Towards the ultimate conservative difference scheme: IV. A new approach to numerical convection, *J. Comput. Phys.*, *23*, 276–299.
- Verver, G. H. L., D. R. Sikka, J. M. Lobert, G. Stossmeister, and M. Zachariasse (2001), Overview of the meteorological conditions and atmospheric transport processes during INDOEX 1999, *J. Geophys. Res.*, *106*, 28,399–28,414.

N. Bellouin, O. Boucher, J.-F. Léon, and M. S. Reddy, Laboratoire d'Optique Atmosphérique, UFR de Physique, CNRS UMR 8518, Université des Sciences et Technologies de Lille, F-59655 Villeneuve d'Ascq Cedex, France. (bellouin@loa.univ-lille1.fr; boucher@loa.univ-lille1.fr; leon@loa.univ-lille1.fr; reddy@loa.univ-lille1.fr)

M. Pham, Service d'Aéronomie, Boîte 102, Université Pierre et Marie Curie, 4 Place Jussieu, F-75252 Paris Cedex 05, France. (mai.pham@aero.jussieu.fr)

C. Venkataraman and S. Verma, Department of Chemical Engineering, Indian Institute of Technology Bombay, Mumbai 400076, India. (chandra@che.iitb.ac.in; shubha@iitb.ac.in)